Verification of Concrete Material Models for MM-ALE Simulations

Swee Hong TAN, Roger CHAN, Jiing Koon POON and David CHNG

Ministry of Home Affairs, Singapore

Abstract

Although there are many concrete material models in LS-DYNA®, very few appear to be valid for Multi-Material Arbitrary Lagrangian-Euler (MM-ALE) simulations. From a rudimentary point of view, it makes sense at the first instance, that the typical method of verification via simulating cylinder tests in triaxial and/or uniaxial stress states for Lagrangian format should work for MM-ALE as well. This paper shares the experiences gathered from attempts at simulating cylinder tests involving MM-ALE concrete material models. Useful insights were gained and they would form part of the considerations for future work.

1. Introduction

There are as many as 30 material models available in LS-DYNA to model geo-materials, such as soil, concrete and rock, listed in reference tables in LS-DYNA Keyword User's Manual Volume II (Material Models) [1]. However, only a small number of them are valid to be used with Multi-Material Arbitrary Lagrangian-Euler (MM-ALE) solid element formulation. According to the document, there are 2 classes of materials which support MM-ALE solid element formulation. They are namely Category 8A which refers to "validated" and Category 8B which refers to "implemented but not validated". With regards to the latter, there is a footnote that advises users to exercise caution as errors associated with advection can arise and may lead to non-physical results, non-conservation of energy and numerical instability.

Initial arbitrary runs involving concrete material models, such as *Mat72R3 (Karagozian & Case (K&C) Concrete Model Release 3), *Mat159 (Continuous Surface Cap Model), *Mat84-85 (Winfrith Concrete Model) and *Mat272 (RHT Concrete Model) were carried out using MM-ALE solid formulation. All these material models have in-built capabilities to auto-generate full suite of parameters including Equation-Of-State (EOS). It was observed that *Mat72R3, unlike the other three materials models (*Mat159, *Mat84-85 and *Mat272), did not result in error termination due to the invalidity of the specific material model for MM-ALE solid elements. This finding came as a surprise, as all the four materials models are neither classified under Category 8A nor 8B. The fact that the simulation involving *Mat72R3 could still run, coupled with the observation that a number of papers had reported the use of *Mat72R3 with MM-ALE solid elements [2, 3], appears to suggest that MM-ALE solid formulation is implemented for *Mat72R3. A possible reason could be that the predecessors of *Mat72R3, such as *Mat16 (Pseudo Tensor) and *Mat72, are currently tagged with Category 8B.

While there is no detailed explanation in the LS-DYNA Keyword User's Manual Volume II (Material Models) with respect to what "validated" exactly entails, a more fundamental issue from a novice user's perspective is how to check whether MM-ALE solid formulation is implemented for the specific material model (in this case, *Mat72R3), besides drawing reference from the document. For Lagrangian formulation, one is able to verify the material model by simulating material model via simple small-scale component tests, such as uniaxial strain and uniaxial stress tests. Here, the same approach using MM-ALE formulation was adopted in an attempt to derive useful insights of the material model.

This paper shares the experiences gathered and compares the results of the simulation runs conducted using both Lagrangian and MM-ALE solid formulation under 2 simple loading conditions, namely uniaxial strain and uniaxial stress, against work hardening calculations based on Incremental Theory of Plasticity [4]. Excel Visual Basic for Applications (VBA) in which the source codes (often referred to as "Macros") were coupled with cell-based programming using formulas and matrix operations was used for the work hardening calculations. No computational grid was considered in Excel VBA which meant that calculations were based on a material point, i.e. an infinitesimal volume element. The purpose of employing VBA was two-fold; first, to check and reinforce understanding of material models and second, to serve as a code verification tool. Two materials models were considered - *Mat72R3 and *Mat5 (Soil & Foam Model). *Mat5 was chosen because it is classified under Category 8A, and also because of its simplicity as a Drucker-Prager algorithm with no strain hardening. As non-local techniques were not incorporated in Excel VBA, no verification on softening could be done. Nevertheless, this paper discusses some preliminary observations on compressive softening based on Lagrangian single element simulations using *Mat72R3 under uniaxial stress loading condition.

2. Motivation

Identifying suitable concrete material models to be used in conjunction with MM-ALE solid formulation is of interest to Ministry of Home Affairs (MHA) Singapore, as part of a long-term technology development programme to study close-in, contact and near contact blast effects on structural elements as well as the mechanism of progressive collapse [5, 6, 7]. Codes for building protection against blast, such as ASCE Standard 59-11 [8], have stipulated that simplified methods such as Pressure-Impulse (PI) charts, Single-Degree-Of-Freedom (SDOF) and/or Multi-Degree-Of-Freedom (MDOF) are not applicable for design and analysis of structural components against close-in, contact and near contact scenarios. Advanced non-linear finite element analyses need to be carried out to assess the near-field blast propagation which is highly non-uniform and to calculate complex structural response modes which cannot be predicted by analytical methodologies. With enhancements to MM-ALE capabilities in LS-DYNA in recent years [9, 10, 11, 12], it is pertinent for MHA to assess the use of associated techniques as a viable alternative to Lagrangian approach, whereby severe hour-glassing due to excessive structural deformations often result in unrealistic energy balances.

3. Material Models

The key parameters for both *Mat5 and *Mat72R3 cards were kept consistent in both uniaxial strain and uniaxial stress loading conditions. Figures 1 & 2 show the respective entries.

For *Mat5, in order to ensure that the uniaxial strain path meets the Drucker-Prager yield criterion, f, pre-set Elastic Bulk Modulus, K_e (13,505 MPa), and Shear Modulus, G (10,554 MPa), were checked against a specific function of the chosen value $\alpha = 0.1$.

$$f = \sqrt{J_2} \pm \alpha I_1 - k$$

$$\frac{2G}{\sqrt{3}K_e} > 3\alpha$$

Adopting chosen value $k = 2.976$ MPa, inputs for a_0, a_1, and a_2 were then determined.

A Plastic Bulk Modulus, K_p (16,305 MPa), along compressive meridian was subsequently calculated from derived incremental relation between hydrostatic pressure and volumetric strain [4]. This completed the basis of the EOS to be entered into the material card. As *Mat5 only allows unloading based on the maximum slope in EOS, the unloading bulk modulus was set to match K_p.

For *Mat72R3, the entire suite of parameters was auto-generated based on unconfined compressive strength of 33.33 MPa. The only modifications done were, first, *slamda* was changed from 100 to 0 so as to be consistent with Excel VBA, and second, the *locwidth* was amended to reflect "three times x maximum aggregate diameter" (3 x 20 mm = 60 mm).

```
*MAT_SOIL_AND_FOAM_TITLE
Mat 5
$#      mid          ro           g        bulk          a0          a1          a2          pc
          1 2.1200E-3       10554       16305      8.8566      1.7856       0.090
$#      vcr         ref        lcid
          0       0.000           0
$#     eps1        eps2        eps3        eps4        eps5        eps6        eps7        eps8
          0 0.0003658 0.0010974    0.001829
$#     eps9       eps10

$#       p1          p2          p3          p4          p5          p6          p7          p8
          0        4.94     16.8692     28.7984
$#       p9         p10
```

Figure 1:   Material Card for *Mat5

```
*MAT_CONCRETE_DAMAGE_REL3_TITLE
Concrete
$     MATID          RO          PR
$#      mid          ro          pr
          1 2.1200E-3    0.190000
$#       ft          a0          a1          a2          b1       omega         a1f
   3.115000    9.855000    0.446300 2.4240E-3    1.600000    0.500000    0.441700
$# slambda        nout       edrop       rsize         ucf       lcrate     locwidth        npts
          0    2.000000    1.000000 3.9720E-2  145.00000           0   60.000000  13.000000
$# lambda1     lambda2     lambda3     lambda4     lambda5     lambda6     lambda7     lambda8
      0.000  8.0000E-6   2.4000E-5   4.0000E-5   5.6000E-5   7.2000E-5   8.8000E-5   3.2000E-4
$#lambda09    lambda10    lambda11    lambda12    lambda13          b3         a0y         a1y
  5.2000E-4  5.7000E-4    1.000000 10.0000001.0000E+10    1.150000    7.441000    0.625000
$#     eta1        eta2        eta3        eta4        eta5        eta6        eta7        eta8
      0.000    0.850000    0.970000    0.990000    1.000000    0.990000    0.970000    0.500000
$#    eta09       eta10       eta11       eta12       eta13          b2         a2f         a2y
   0.100000       0.000       0.000       0.000       0.000    1.350000   3.5480E-3   7.7230E-3
```

```
*EOS_TABULATED_COMPACTION_TITLE
Concrete
$    EOSID     Gamma        E0       Vol0
$#   eosid      gama        e0         vo
         8     0.000     0.000   1.000000
$#         ev1              ev2              ev3              ev4              ev5
         0.000  -1.500000e-003  -4.300000e-003  -1.010000e-002  -3.050000e-002
$#         ev6              ev7              ev8              ev9             ev10
  -5.130000e-002  -7.260000e-002  -9.430000e-002       -0.174000       -0.208000
$#          c1               c2               c3               c4               c5
         0.000       22.042049       48.051670       77.147171      146.579636
$#          c6               c7               c8               c9              c10
    221.081757      313.658356      479.855438     2801.544434     4284.974121
$#          t1               t2               t3               t4               t5
         0.000           0.000           0.000           0.000           0.000
$#          t6               t7               t8               t9              t10
         0.000           0.000           0.000           0.000           0.000
$#          k1               k2               k3               k4               k5
  14690.000000    14690.000000    14900.000000    15650.000000    18620.000000
$#          k6               k7               k8               k9              k10
  21600.000000    24570.000000    26820.000000    60340.000000    73470.000000
```

Figure 2:   **Material & EOS Cards for *Mat72R3**

4. Uniaxial Strain

Figure 3 illustrates the various configurations for simulation under uniaxial strain loading condition. They were single element (20 mm) and multi-element set-ups (in the form of cylinder that measured 300 mm height by 150 mm in diameter), adopting either Lagrangian or MM-ALE solid formulation. At both extreme ends of the MM-ALE cylinder, Lagrangian shell elements were created to impose the required prescribed boundary displacements via the common Lagrangian nodes with the MM-ALE part. Unloading was set near 0.1% and 0.5% strain for *Mat5 and *Mat72R3 respectively. The strain rate was kept very low, at 1e-5 per ms throughout, so as to simulate a near quasi-static response without inducing unnecessary inertia confinement effects [13]. The solver employed was R6.1.1 SMP Double Precision.

Figures 4 & 5 compare the calculations from Excel VBA against simulation results for *Mat5 and *Mat72R3 respectively. The outputs for the cylinders were extracted via *DATABASE_ELOUT. It was observed that for both Lagrangian and MM-ALE cylinders, results were identical throughout all elements. Therefore, averaging of results was not necessary for plotting.

The calculations from Excel VBA had tallied almost perfectly with simulation results for both *Mat5 and *Mat72R3. In particular for *Mat72R3, not only the deviatoric and volumetric responses were well captured, the modified effective plastic strain value, λ, matched plots from LS-DYNA, extracted via "history var#6" written by setting NEIPH=6 on the keyword *DATABASE_EXTENT_BINARY.

While Excel VBA for *Mat5 had followed the analytical expressions for Drucker-Prager material, the incremental relations for *Mat72R3 were derived from first principles [4], and in accordance to documentation by K&C [14, 15, 16, 17, 18]. The shear modulus correction procedure based on scaled bulk modulus was also included for the unloading path. The key computations in Excel VBA for *Mat72R3 via a "FOR" loop are summarized as follows.

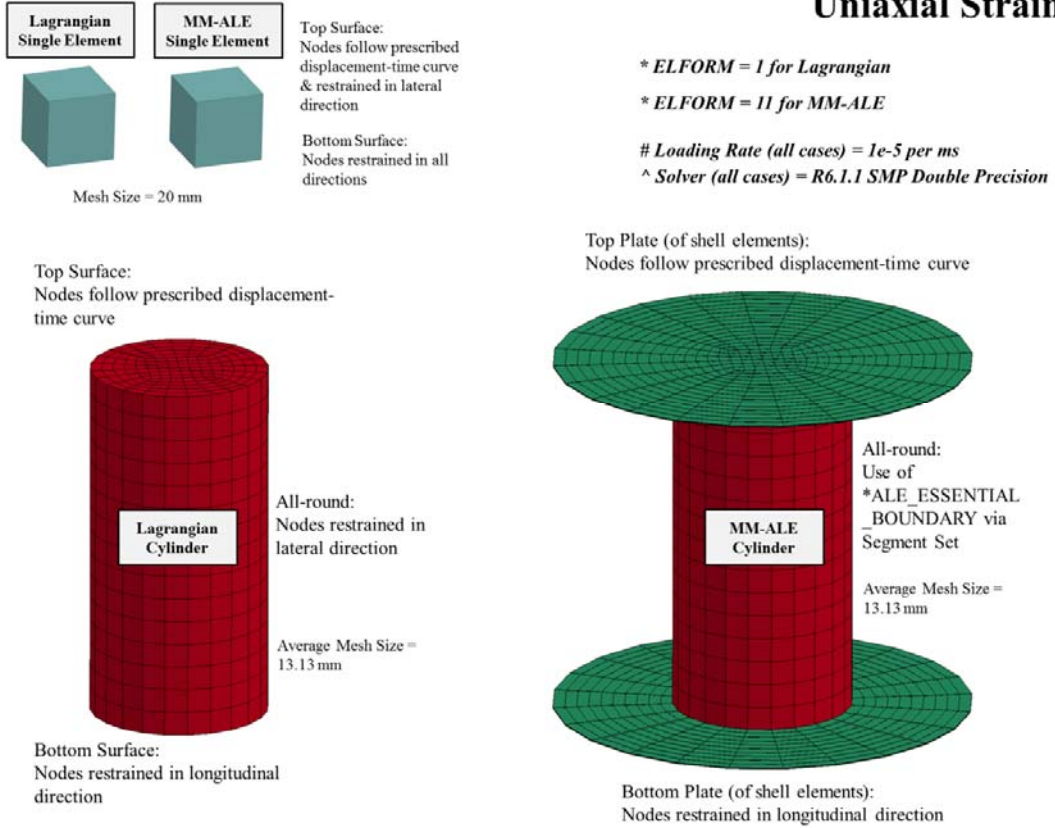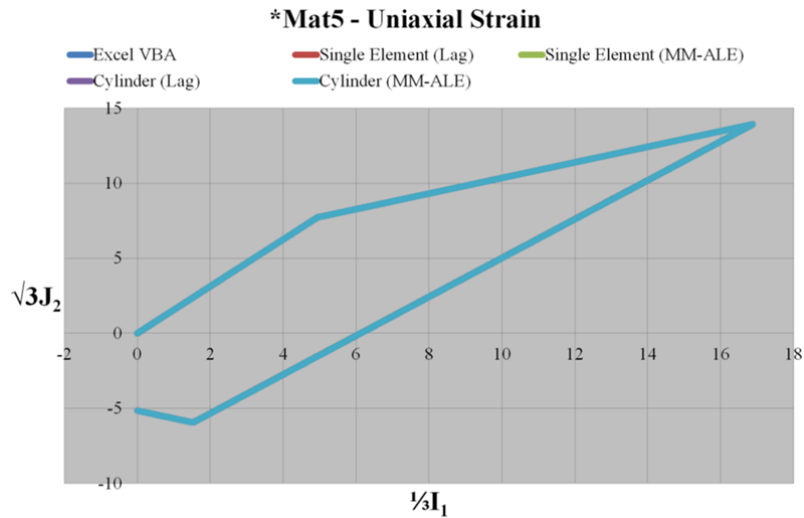**Figure 3:** **4 configurations subjected to uniaxial strain loading condition**
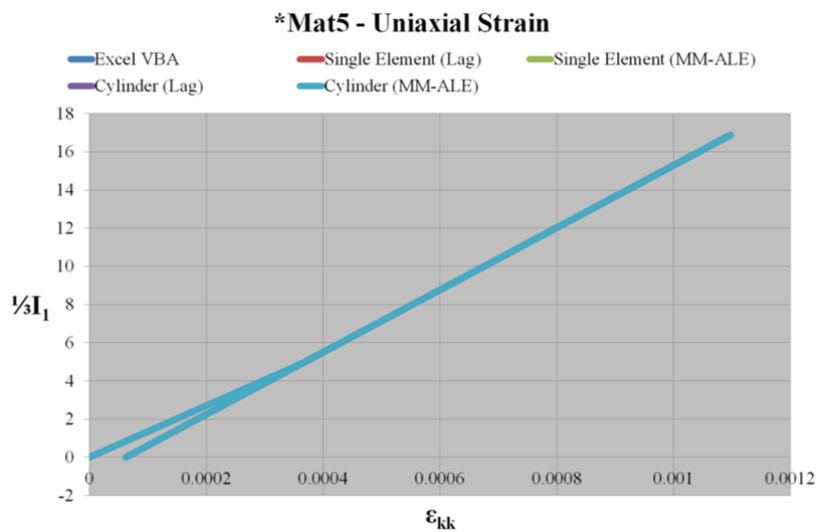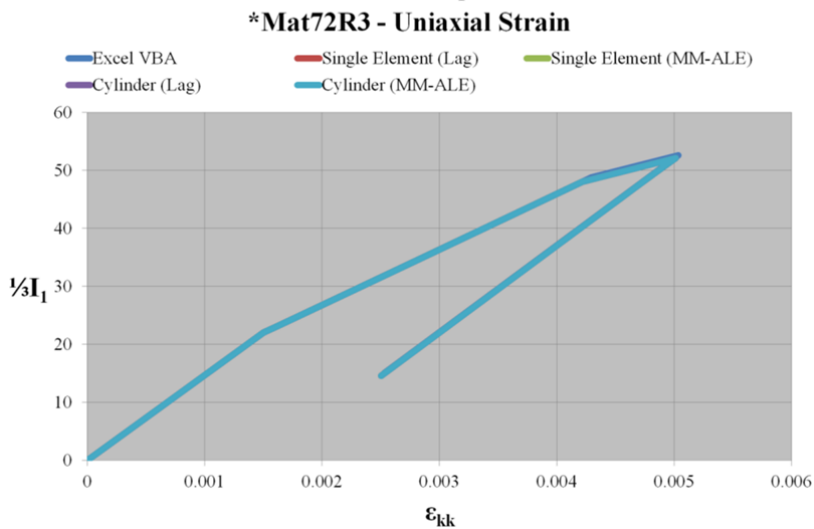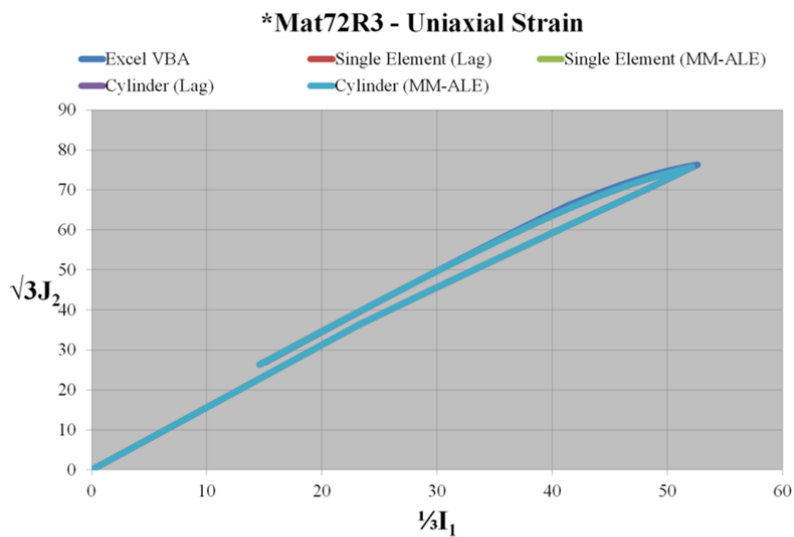
*Mat5 - Uniaxial Strain

Figure 4a & b: Plots of results for *Mat5 under uniaxial strain loading condition

*Mat72R3 - Uniaxial Strain

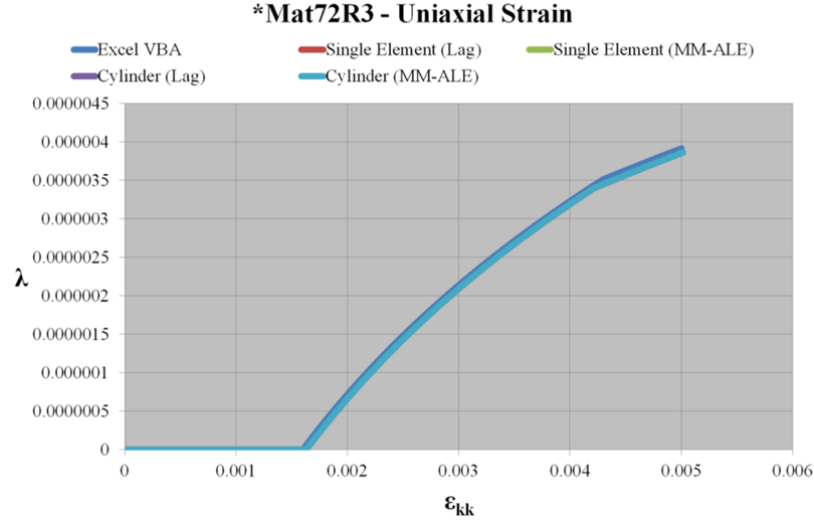***Mat72R3 - Uniaxial Strain**

*Mat72R3 - Uniaxial Strain

Figure 5a, b & c: **Plots of results for *Mat72R3 under uniaxial strain loading condition**

Plastic Potential, *G*

$$G = \sqrt{3J_2} - \omega\left[\eta\left(\Delta\sigma_m - \Delta\sigma_y\right) + \Delta\sigma_y\right]$$

where ω & η represent the extent of associativity and interpolation parameter respectively, and

$$\Delta\sigma_m = a_0 + \cfrac{\cfrac{I_1}{3}}{a_1 + a_2\cfrac{I_1}{3}}$$

$$\Delta\sigma_y = a_{0y} + \cfrac{\cfrac{I_1}{3}}{a_{1y} + a_{2y}\cfrac{I_1}{3}}$$

Failure Function, *F*

$$F = \sqrt{3J_2} - \left[\eta\left(\Delta\sigma_m - \Delta\sigma_y\right) + \Delta\sigma_y\right]$$

Scalar Proportionality Factor

$$d\mu = \cfrac{\cfrac{\partial F}{\partial\sigma_{ij}}{D_{ijkl}}^e d\varepsilon_{kl}}{9\omega K\left(\cfrac{\partial F}{\partial I_1}\right)^2 + 3G + \left(\cfrac{\partial F}{\partial\eta}\right)\left(\cfrac{\partial\eta}{\partial\lambda}\right)h(\sigma_{ij})\sqrt{2\left(\cfrac{\partial G}{\partial I_1}\right)^2 + 1}}$$

$$h(\sigma_{ij}) = \cfrac{1}{\left(1 + \cfrac{p}{f_t}\right)^{b_1}}$$

$$d\lambda = h(\sigma_{ij})\sqrt{\left(\cfrac{2}{3}\right)d\varepsilon_{ij}^p d\varepsilon_{ij}^p}$$

where p, f_t, b_1, K & G represent pressure, uniaxial tensile strength, compressive damage scaling parameter, bulk and shear modulus respectively

4th order elastic-plastic tensor

$$D_{ijkl}{}^{ep} = D_{ijkl}{}^{e} - \frac{A_{ij}B_{kl}}{H}$$

where A_{ij} and B_{kl} are 2nd order tensors as functions of $\frac{\partial G}{\partial I_1}$, $\frac{\partial G}{\partial J_2}$ and $\frac{\partial F}{\partial I_1}$, $\frac{\partial F}{\partial J_2}$ respectively, with K, G & Deviatoric Stress, s_{ij}, while H is a scalar function involving all terms except s_{ij}

Stress-Strain Incremental Relation

$$d\sigma_{ij} = D_{ijkl}{}^{ep} d\varepsilon_{kl}$$

5. Uniaxial Stress

Figure 6 illustrates the various configurations for simulation under uniaxial stress loading condition. They were largely similar to that used in uniaxial strain loading condition except for a couple of differences. Firstly, the nodal constraints along the longitudinal axis for all single elements and Lagrangian cylinder were released, and secondly, MM-ALE air elements were created around MM-ALE cylinders to allow for radial expansion, in replacement of *ALE_ESSENTIAL_BOUNDARY. An additional MM-ALE cylinder of reduced average mesh of 6.4 mm was also included. No unloading was stipulated.

Figures 7 and 8 compare the calculations from Excel VBA against simulation results for *Mat5 and *Mat72R3 respectively. Unlike uniaxial strain case, it was observed that only the Lagrangian cylinder had identical results across all elements. Both coarse and fine mesh MM-ALE cylinders had varying results across all elements.

For MM-ALE cylinders, an important point to take note is that the contributions from the two outermost circumferential layers of elements, as illustrated in Figure 9, were not included for averaging. The outermost circumferential layer of elements had contained some volume fraction of air. This was normal, as all interface elements between two MM-ALE materials in LS-DYNA would, by default, contain the fluid interface around which the volume fractions would be graded towards both sides. The reason behind the omission of the 2nd outermost circumferential layer of elements for averaging, was due to an observed "sharp discontinuity" in modified effective plastic strain value, λ, output in *Mat72R3 MM-ALE cylinders between the 2nd and 3rd outermost circumferential layer of elements. To be consistent with *Mat72R3, the same was carried out for *Mat5.

The calculations from Excel VBA only matched well with simulation results from the single elements and the Lagrangian cylinder for both *Mat5 and *Mat72R3, but not for the MM-ALE cylinders. This was unlike earlier uniaxial strain cases, whereby calculations from Excel VBA had tallied almost perfectly with simulation results of all configurations including MM-ALE cylinders.

For *Mat5 MM-ALE cylinders, it appeared that the LS-DYNA computation for coarse mesh cylinder had encountered error at about 0.17% strain as it had exhibited strain hardening which was totally unexpected of the Drucker-Prager algorithm. Conversely, the fine mesh cylinder had yielded reasonable results although the effective stress declined initially before reaching steady state at approximately about 10% below theoretical value. The likely reason behind the drop could be the advection of concrete material into air.
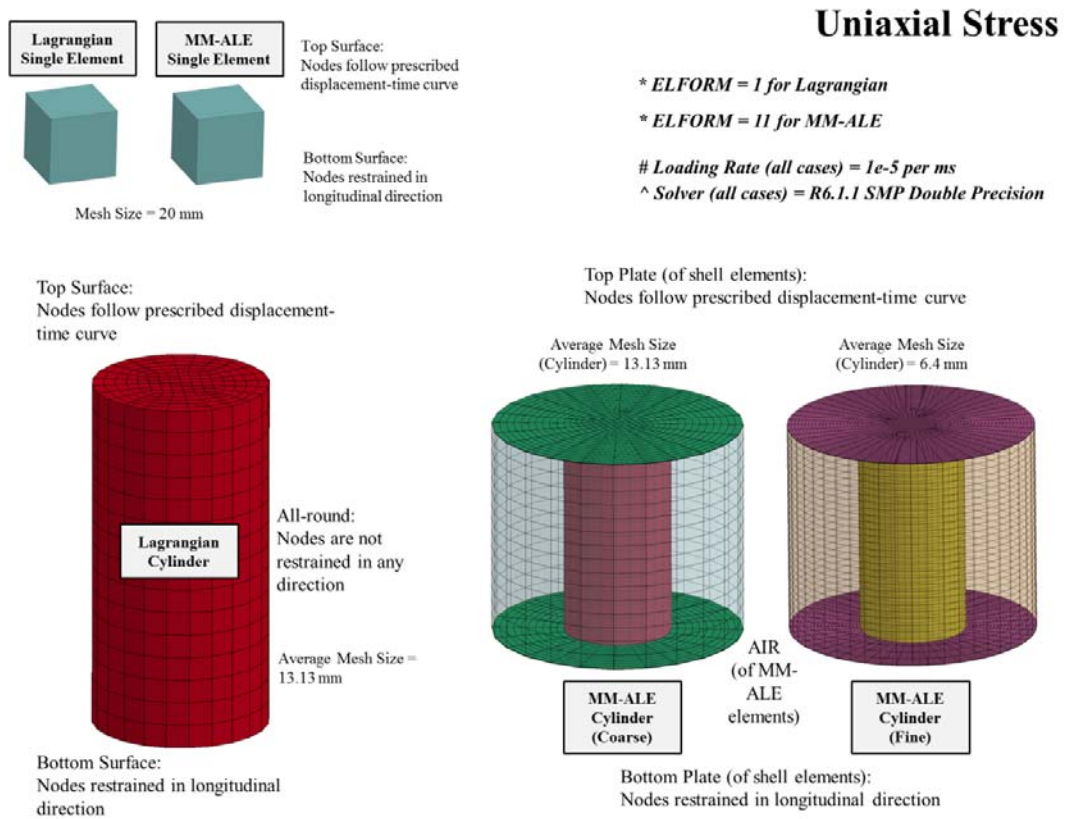
Figure 6: 5 configurations subjected to uniaxial stress loading condition
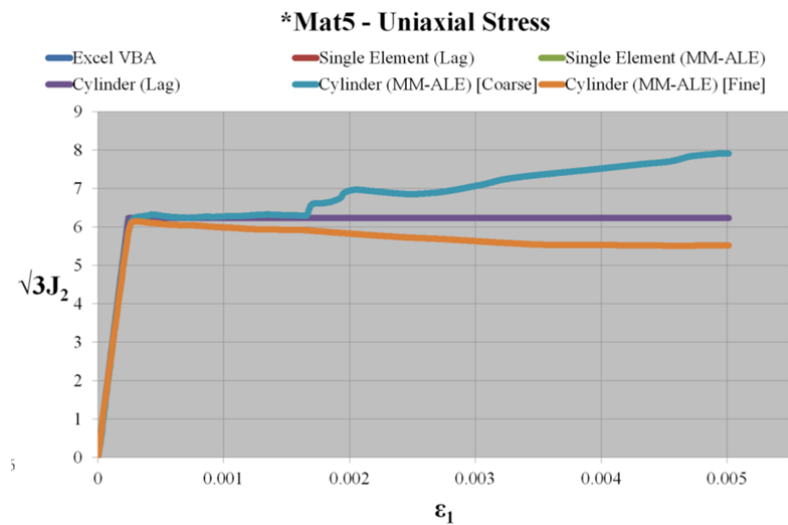

Figure 7: Plots of results for *Mat5 under uniaxial stress loading condition
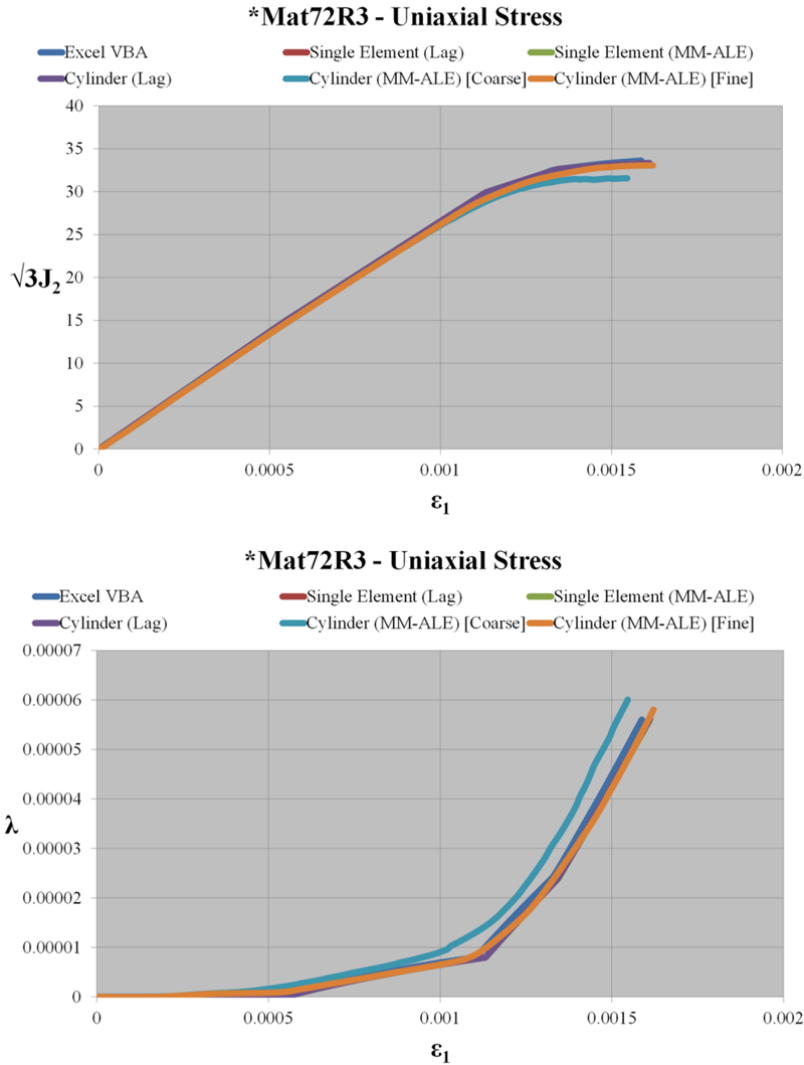
Figure 8a & b: Plots of results for *Mat72R3 under uniaxial stress loading condition
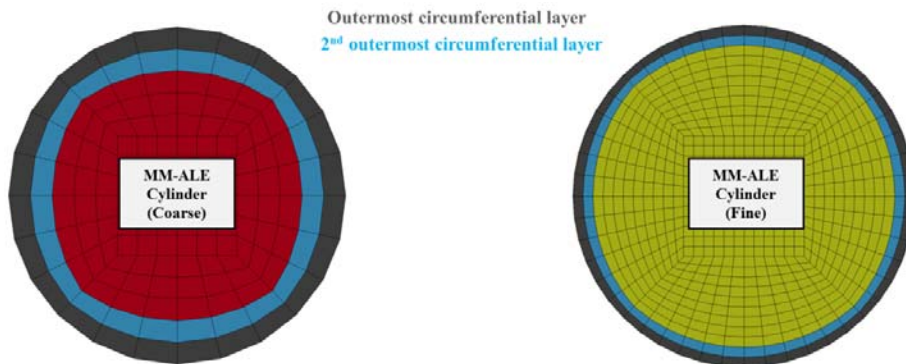

Figure 9:   Illustration of the Two Outermost Circumferential Layers for MM-ALE Cylinders

For *Mat72R3 MM-ALE cylinders, it was clear that the fine mesh cylinder had performed better than the coarse mesh counterpart. Unlike uniaxial strain loading condition, the computations for *Mat72R3 in Excel VBA could no longer driven by total strain in a straightforward manner. Various plastic strain quantities were unknown and hence total strain could not be established deterministically. More specifically, the numerator of Scalar Proportionality Factor had to be substituted with an equivalent expression via Taylor series expansion to enact the concept of trial elastic stress state and the numerical implementation had to be in the form of "radial return". A small enough elastic strain increment along the principal loading axis, $\Delta\varepsilon^e$, had to be selected by user to achieve good convergence of results. The key computations in Excel VBA for *Mat72R3 via a "DO… IF" loop are summarized as follows.

Numerator of Scalar Proportionality Factor

$$\frac{\partial F}{\partial \sigma_{ij}} D_{ijkl}{}^e d\varepsilon_{kl} = \frac{\partial F}{\partial \sigma_{ij}} (d\sigma^*) \cong F(\sigma_n + d\sigma^*) \cong F(\sigma^*)$$

$$F(\sigma^*) = \sqrt{3{J_2}^*} - Y^*$$

where $d\sigma^*$, σ_n & σ^* represent the trial elastic stress increment, current stress state and trial stress state respectively, and Y^* denotes the yield surface, i.e. $[\eta(\Delta\sigma_m - \Delta\sigma_y) + \Delta\sigma_y]$, evaluated at current value of modified effective plastic strain value, λ, with trial stress state

Elastic Volumetric Strain Increment

$$\Delta\varepsilon^e_{kk} = (1 - 2v)\Delta\varepsilon^e$$

Deviatoric Strain Increments

$$\Delta e_1 = \Delta\varepsilon^e - \frac{1}{3}(1 - 2v)\Delta\varepsilon^e$$

$$\Delta e_2 = \Delta e_3 = -v\Delta\varepsilon^e - \frac{1}{3}(1 - 2v)\Delta\varepsilon^e$$

Trial Deviatoric Stresses

$$s_{trial} = s_n + 2G\Delta e$$

where s_n represents current deviatoric stress

Trial Pressure

$$p^* = K(\varepsilon^e_{kk} + \Delta\varepsilon^e_{kk})$$

where ε^e_{kk} represents current elastic volumetric strain

With s_{trial} and p^*, $\sqrt{3{J_2}^*}$ and Y^* can be calculated. The same applies to the denominator of the Scalar Proportionality Factor. This completes computation of $d\mu$ and $d\lambda$.

New Yield Surface

$$Y_{n+1} = Y^* + \left(\frac{\partial Y}{\partial I_1}\right) dI_1{}^p + \left(\frac{\partial Y}{\partial \eta}\right)\left(\frac{\partial \eta}{\partial \lambda}\right) d\lambda$$

where $dI_1{}^p = d\mu \left(9K\omega \frac{\partial Y}{\partial I_1}\right)$ and "*n+1*" denotes updated state

Scaling of Deviatoric Stress to New Yield Surface

$$s_{n+1} = \left(\frac{Y_{n+1}}{\sqrt{3J_2{}^*}}\right) s_{trial}$$

Updates to *p* and *λ*,

$$p_{n+1} = p^* + \frac{dI_1{}^p}{3}$$

$$\lambda_{n+1} = \lambda_n + d\lambda$$

New Stress & Strain (along principle loading axis)

$$\sigma_{n+1} = s_{n+1} + p_{n+1}$$

$$\varepsilon_{n+1} = \varepsilon_n + \Delta\varepsilon^e + \Delta\varepsilon^p = \varepsilon_n + \Delta\varepsilon^e + d\mu \left(\frac{\partial G}{\partial I_1} + \frac{\partial G}{\partial J_2} s_{trial\,(1)}\right)$$

where $\Delta\varepsilon^p$ and $s_{trial\,(1)}$ denote the plastic strain increment and trial deviatoric stress along principle loading axis respectively

Figure 10a illustrates the observed "sharp discontinuity" in modified effective plastic strain value, λ, output in *Mat72R3 MM-ALE cylinders between the 2ⁿᵈ and 3ʳᵈ outermost circumferential layer of elements, while Figure 10b shows the corresponding effective stress plots.

It was apparent that the 2ⁿᵈ outermost circumferential layer of elements for both coarse and fine mesh MM-ALE cylinders, despite having full volume of concrete, had encountered overwhelmingly large values of λ compared to those elements located within 3ʳᵈ outermost layer. Considering that the materials at the 2ⁿᵈ outermost circumferential layer of elements could either be at the onset or in the process of advection, one possible explanation was that the advection algorithm (if any) was lacking in damage calculations. In practical sense, it could mean that as long as *Mat72R3 material moves across the grid, even if the extent is small, damage gets accumulated unrealistically fast. From observation, this phenomenon was numerical as it depended on the mesh size employed.

On the other hand, the peak stresses recorded had shown only minimal differences, and hence had appeared to be independent of whether the 2ⁿᵈ outermost circumferential layer was considered for averaging. This was expected since the number of elements in that layer that experienced extremely high modified effective plastic strain values was only a small fraction of the total number of elements. Extremely high values of λ would imply low strength performance of those elements in the 2ⁿᵈ outermost circumferential layer. The resulting disparity in effective strengths would not be as great as compared to that in λ.
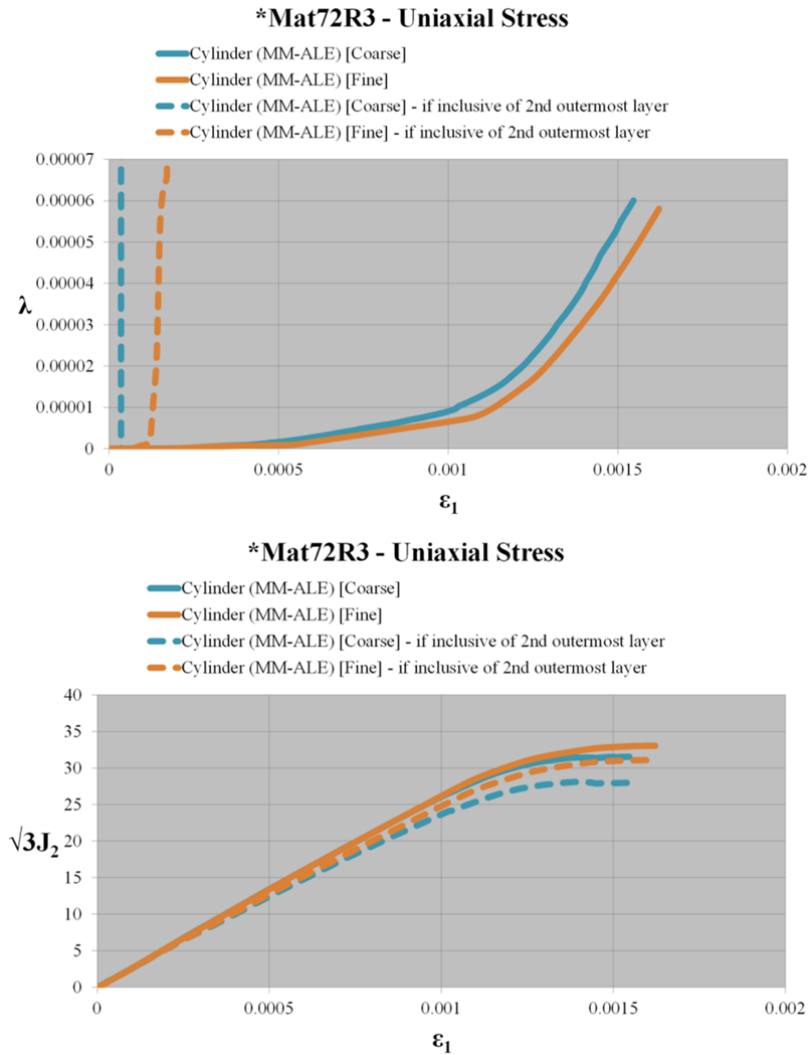
*Mat72R3 - Uniaxial Stress

Cylinder (MM-ALE) [Coarse]
Cylinder (MM-ALE) [Fine]
Cylinder (MM-ALE) [Coarse] - if inclusive of 2nd outermost layer
Cylinder (MM-ALE) [Fine] - if inclusive of 2nd outermost layer

*Mat72R3 - Uniaxial Stress

Cylinder (MM-ALE) [Coarse]
Cylinder (MM-ALE) [Fine]
Cylinder (MM-ALE) [Coarse] - if inclusive of 2nd outermost layer
Cylinder (MM-ALE) [Fine] - if inclusive of 2nd outermost layer

Figure 10a & b: Observed "sharp discontinuity" in λ between the 2nd and 3rd outermost circumferential layer of elements and corresponding effective stress plots for *Mat72R3 MM-ALE cylinders

6. Compressive Softening

While regularization for tensile softening based on fracture energy considerations was explained and demonstrated in details [16], there is little information from open source literature with regards to regularization for compressive softening in *Mat72R3. Several Lagrangian single element simulations under uniaxial stress loading condition, involving varying mesh sizes and inputs of *locwidth*, were carried out. Figure 11 had revealed trends similar to tensile softening, i.e. as long as the mesh size was higher than stipulated localization width, plots of strain energy per displacement (which was obtained by integrating the stress versus displacement response for each element) against the displacement would be identical. This could imply that the same technique for tensile softening was adopted for compressive softening in *Mat72R3. However, the technique behind regularization for tensile softening in *Mat72R3 is Crack Band Theory, which was earlier developed to address only Mode I fracture, i.e. opening mode whereby tensile stress is normal to plane of the crack [19]. Hence, it may not be appropriate to adopt the same for compressive softening. Other methodologies such as non-local integral or gradient formulations [20] may be more suitable. It was later found out from [18], that K&C has plans to look into this area.
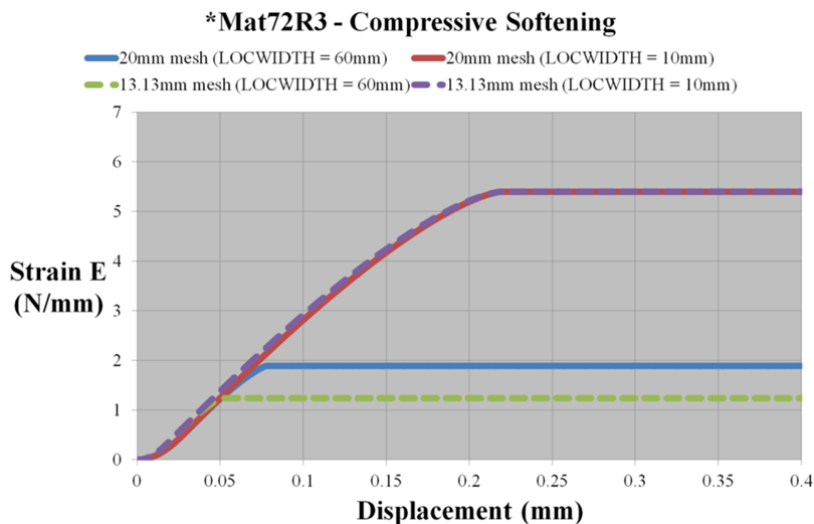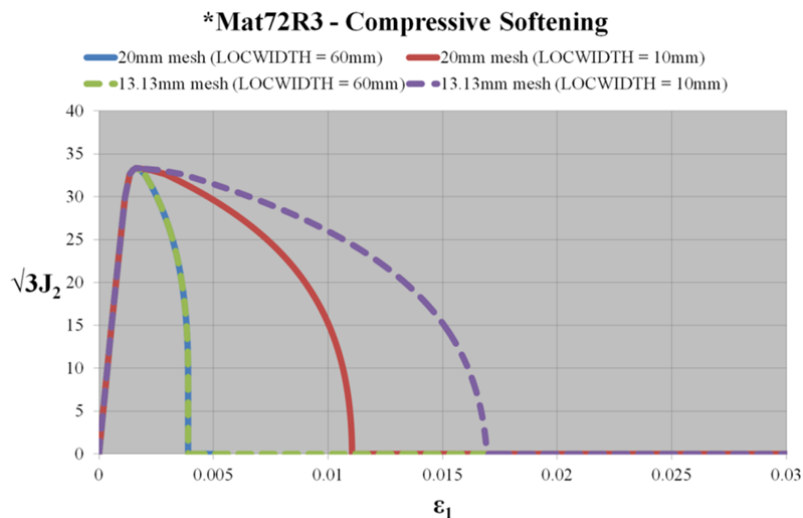
Figure 11a & b: Lagrangian single element simulations under uniaxial stress loading condition, involving varying mesh sizes and inputs of *locwidth*

7. Conclusion

Although the uniaxial strain and uniaxial stress models had not involved large extent of advection as compared to typical MM-ALE applications, useful insights were gained. It was established that, damage in *Mat72R3 can get accumulated unrealistically fast as soon as slight movement of material is detected. While this can be acceptable in one-off simulations of scenarios such as penetration etc., in which material is expected to undergo substantial deformation and fail catastrophically, extra care needs to be exercised in other simulations if assessment of residual strength of the damaged material is required, such as those of columns subjected to blast etc. These learning points would form part of the considerations for future work.

8. References

[1]   LS-DYNA 971 R7.0 Keyword User's Manual II, 2013

[2]   Len Schwer. "Penetration and Perforation Simulation Techniques: Lagrange with Erosion, Smooth Particle Hydrodynamics and Multi-Material Arbitrary Lagrange Eulerian", 13ᵗʰ International Symposium on Interactions of the Effects of Munitions on Structures (ISIEMS), 2009

[3]   John M. H. Puryear, David J. Stevens, Kirk A. Marchand, Eric B. Williamson, C. Kennan Crane. "ALE Modeling of Explosive Detonation on or near Reinforced-Concrete Columns", 12ᵗʰ International LS-DYNA Users Conference, 2012

[4]   Wai Fah Chen. "Plasticity in Reinforced Concrete", 2007

[5]   Swee Hong Tan, Jiing Koon Poon, Roger Chan, David Chng. "Retrofitting of Reinforced Concrete Beam-Column via Steel Jackets against Close-in Detonation", 12ᵗʰ International LS-DYNA Users Conference, 2012

[6]   Swee Hong Tan, Shih Kwang Tay, Jiing Koon Poon, David Chng. "Fluid-Structure Interaction involving Close-in Detonation Effects on Column using LBE MM-ALE Method", 9ᵗʰ European LS-DYNA Users Conference, 2013

[7]   Jiing Koon Poon, Roger Chan, David Chng. "Contact and Near-Contact Detonation on Concrete Components", 15ᵗʰ International Symposium on Interactions of the Effects of Munitions on Structures (ISIEMS), 2013

[8]   ASCE Standard 59-11. Blast Protection of Buildings, 2011

[9]   Slavik, T. "A Coupling of Empirical Explosive Blast Loads to ALE Air Domains in LS-DYNA", 7ᵗʰ European LS-DYNA Users Conference, 2009

[10]   Nicolas Aquelet, Mhamed Souli. "2D to 3D Mapping", 10ᵗʰ International LS-DYNA Users Conference, 2010

[11]   Nicolas Aquelet. "ALE Adaptive Mesh Refinement in LS-DYNA", 12ᵗʰ International LS-DYNA Users Conference, 2012

[12]   Hao Chen, Jason Wang. "LS-DYNA ALE Nodal Coupling", 12ᵗʰ International LS-DYNA Users Conference, 2012

[13]   Len Schwer. "Strain Rate Induced Strength Enhancement in Concrete: Much ado about Nothing?", 7ᵗʰ European LS-DYNA Users Conference, 2009

[14]   L. J. Malvar, D. Simons. "Concrete Material Modeling in Explicit Computations", Workshop on Recent Advances in Computational Structural Dynamics and High Performance Computing, 1996

[15]   L. J. Malvar, J. E. Crawford, J. W. Wesevich, D. Simons. "A Plasticity Concrete Material Model for DYNA3D", International Journal of Impact Engineering, Volume 19, no. 9/10, December 1997, pp. 847-873

[16]   Joseph M. Magallanes, Youcai Wu, L. Javier Malvar, John E. Crawford. "Recent Improvements to Release III of the K&C Concrete Model", 11ᵗʰ International LS-DYNA Users Conference, 2010

[17]   Youcai Wu, John E. Crawford, Joseph M. Magallanes. "Performance of LS-DYNA Concrete Constitutive Models", 12ᵗʰ International LS-DYNA Users Conference, 2012

[18]   John E. Crawford, Youcai Wu, Hyung-Jin Choi, Joseph M. Magallanes, Shengrui Lan. "Use and Validation of the Release III K&C Concrete Material Model in LS-DYNA", TR-11-36.5, 2012

[19]   Zdenek P. Bazant, B. H. Oh. "Crack Band Theory for Fracture of Concrete", Materials and Structures, Volume 16, 1983, pp. 155-177

[20]   L. H. Poh, Somsak Swaddiwudhipong. "Over-Nonlocal Gradient Enhanced Plastic-Damage Model for Concrete", International Journal of Solids and Structures, Volume 46, 2009, pp. 4369-4378